JACS
JOURNAL OF THE AMERICAN CHEMICAL SOCIETY

COMMUNICATION

pubs.acs.org/JACS

Plasmonic Gold Nanocrosses with Multidirectional Excitation and Strong Photothermal Effect

Enyi Ye,[†] Khin Yin Win,[†] Hui Ru Tan,[†] Ming Lin,[†] Choon Peng Teng,[†] Adnen Mlayah,*[,‡] and Ming-Yong Han*[,†,§]

[†]Institute of Materials Research and Engineering, Agency for Science, Technology and Research, 3 Research Link, Singapore 117602

[‡]Centre d'Elaboration de Matériaux et d'Etudes Structurales, CNRS-Université de Toulouse, 29 Rue Jeanne Marvig, 31055 Toulouse, France

[§]Division of Bioengineering, National University of Singapore, 9 Engineering Drive 1, Singapore 117576

Supporting Information

ABSTRACT: We report a facile chemical synthesis of well-defined gold nanocrosses through anisotropic growth along both ⟨110⟩ and ⟨001⟩, whereas gold nanorods grow only along either ⟨110⟩ or ⟨001⟩. The multiple branching was achieved by breaking the face-centered-cubic lattice symmetry of gold through copper-induced formation of single or double twins, and the resulting gold nanocrosses exhibited pronounced near-IR absorption with a great extension to the mid-IR region. As studied by discrete dipole approximation (DDA) simulations, the entire nanocross gets excited even when one of the branches is exposed to incident light. The above properties make them useful as octopus antennas for capturing near-IR light for effective photothermal destruction of cells. The cell damage process was analyzed using the Arrhenius model, and its intrinsic thermodynamic characteristics were determined quantitatively. Besides effective photothermal treatment and two-photon luminescence imaging, the near- and mid-IR-absorbing gold nanocrosses may also find applications in IR sensing, thermal imaging, telecommunications, and the like.

Surface plasmons propagate on the surface of metals (silver, gold, palladium, etc.) whose optical properties are determined by their surface geometry at the nanoscale. Recent advancements in controlling the surface shape/morphology of metal nanostructures have demonstrated the great capability to engineer their localized surface plasmon resonance (LSPR).[1] For the LSPR to be tuned from the visible to the near-IR, metal nanostructures must have a size comparable to the optical wavelength in one or more dimensions. For example, metal nanorods, nanoprisms, and nanoplates have red-shifted LSPR as a result of increases in length or edge size,[2] and metal nanoshells, nanorings, and nanocages have red-shifted LSPR when the core/cavity diameter and shell thickness are changed.[3,4] Recently, the successful fabrication of structurally more complex metal nanostructures, including semishells, multishells, split rings, helixes, and gammadions, has produced greatly enriched surface plasmonic properties,[5,6] and the formation of closely spaced arrays of various metal nanostructures on substrates can further enhance these properties through interparticle coupling.[7] In this paper, we report a facile chemical synthesis of free-standing multiple-branched gold nanocrosses, which exhibit a pronounced near- and mid-IR LSPR. The colloidal production of such well-defined gold nanocrosses in a controlled fashion was a challenging task because of the symmetric face-centered-cubic lattice of gold, and the copper-induced formation of single or double twins in the center of the gold nanocrosses in this research was important in determining the unique habit of the final morphology (e.g., D_{2h} or C_{2v} symmetry). Theoretical investigations indicate that an entire nanocross can get excited along any branch and that these plasmonically coupled branches lead to synergistic enhancement of local electric fields,[8] enabling applications in sensing, surface-enhanced spectroscopy, nonlinear optics, imaging, therapeutics, and medicine.[3,5,9] For example, the highly branched gold nanocrosses exhibited a strong photothermal effect for effective photothermal destruction of cells, and this can be integrated with two-photon luminescence imaging to understand the cell damage process for tumor therapies.

Gold nanocrosses were synthesized in oleylamine containing heat-pretreated copper(I) chloride together with gold chloride [see the Supporting Information (SI) for experimental details]. Figure 1 shows a transmission electron microscopy (TEM) image (Figure 1a) and an X-ray diffraction (XRD) pattern (Figure 1b) of phase-pure gold nanocrosses containing 0.86 mol % copper (ICP−AES data are provided in the SI). High-angle annular dark-field scanning transmission electron microscopy (HAADF-STEM) was used to collect 91 images of a single nanocross (Figure 1c) at different specimen orientations for reconstruction of its three-dimensional tomography with front, side, and back views (Figures 1d−f; also see movie S1 in the SI). Figure 2 shows TEM images of two gold nanocrosses, one with D_{2h} symmetry (Figure 2a) and the other with C_{2v} symmetry (Figure 2c), that have single or double twins in their centers, as revealed by the high-resolution TEM (HRTEM) images in Figure 2b,d, respectively. For the doubly twinned nanocross viewed along the $[1\bar{1}0]$ zone axis (Figure 2a), the lattice direction remains the same before and after the twin boundaries (Figure 2b), as shown by one set of selected-area electron diffraction (SAED) spots (Figure 2a inset). For the singly twinned nanocross viewed along the $[1\bar{1}0]$ zone axis (Figure 2c), the lattice direction changes after the twin boundary. Two sets of SAED spots were

Received: April 7, 2011
Published: May 12, 2011

dx.doi.org/10.1021/ja202832r | J. Am. Chem. Soc. 2011, 133, 8506–8509

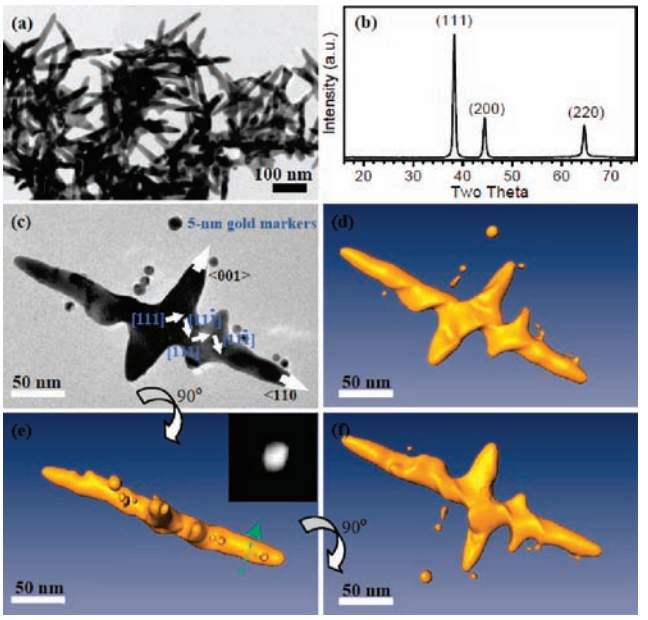

Figure 1. (a) TEM image, (b) XRD pattern, and (c) HAADF-STEM image of a single nanocross. In (c), very small gold nanoparticles were used as markers to view the nanocross in three dimensions. (d–f) Surface-rendered views of the nanocross reconstructed by HAADF-STEM tomography: (d) front view; (e) side view; (f) back view. The inset in (e) displays the cross section of a longer branch of the gold nanocross.

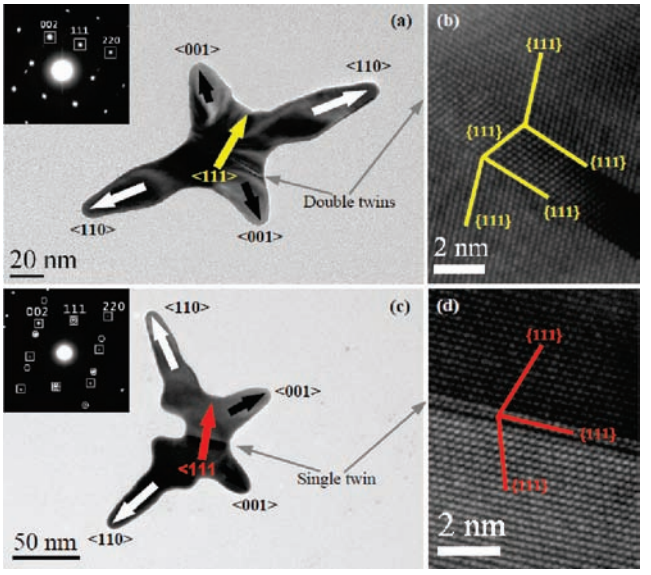

Figure 2. Structural analysis of gold nanocrosses. (a) Low-magnification TEM and (b) HRTEM images of a doubly twinned gold nanocross with D_{2h} symmetry. The inset in (a) shows one set of SAED spots. (c) Low-magnification TEM and (d) HRTEM images of a singly twinned gold nanocross with C_{2v} symmetry. The inset in (c) shows two sets of SAED spots, labeled with squares and circles.

accordingly observed (Figure 2c inset), corresponding to the lower and upper halves of the nanocross, which have different lattice arrangements (Figure 2d).

In both the singly and doubly twinned gold nanocrosses, the two longer branches extend along ⟨110⟩ while the two shorter branches extend along ⟨001⟩. The simultaneous growth along the two directions led to two-dimensional (2D) growth of four-branched gold nanostructures, which is different from conventional 1D growth of gold nanorods along either ⟨110⟩ or ⟨001⟩. The branched gold nanocrosses were formed in the presence of the copper(I) precursor, while only spherical nanoparticles[10] were formed in the absence of copper(I) precursor. This is attributed to the copper-induced formation of single or double twins that may break the cubic lattice symmetry of gold, resulting in the anisotropic growth along both ⟨110⟩ and ⟨001⟩. Four more gold nanocrosses are shown in Figure 3a. The secondary branching growth led to the formation of 3D gold nanocrosses, as shown in panel ④ in Figure 3a.

The near- and mid-IR absorption spectra of gold nanocrosses are shown in Figure 3b,c. A typical gold nanocross (panel ③ in Figure 3a) was chosen as a model for the simulation of the absorption spectrum using the discrete dipole approximation (DDA) (see the SI for details). The average simulated absorption spectrum of the model nanocross [Figure 3d(i)], which was obtained by considering five orientations with respect to the polarization of the excitation light [Figure 3e(ii–vi)], is in good agreement with the measured absorption spectrum (Figure 3b).

With the pronounced near-IR absorption in the biological window (Figure 3c), the gold nanocrosses can serve as efficient absorbers for photothermal destruction of living cells upon near-IR irradiation (Figure S1 in the SI). Experimentally, human lung cancer cells (A549) associated with gold nanocrosses (Figure S2a) died very rapidly within 30 s upon 900 nm laser irradiation at ~4.2 W/cm^2 (Figure S2b, using a 60× objective). The laser-exposed dead cells were imaged at a lower magnification (10×) to show the surrounding live cells beyond the laser-exposed area, illustrating the effect of the localized photothermal treatment (Figure S2c). Control experiments showed that all of the cells that were not associated with gold nanocrosses (Figure S2d) remained alive after laser irradiation at ~4.2 W/cm^2 for 5 min (Figure S2e) and 10 min (Figure S2f).

To analyze the hyperthermia process, cancer cells associated with gold nanocrosses were irradiated with the 900 nm laser at intensities of 1.3, 2.6, and 4.2 W/cm^2. The percentage of dead cells in the laser focus area depended both on the laser intensity and the exposure time (Figure 4a). As shown in movies S2 and S3, all of the cancer cells were destroyed under laser irradiation within 30 s at 4.2 W/cm^2, and ~95% of the cells were killed after laser irradiation for 150 s at 2.6 W/cm^2. The time-dependent damage process at 2.6 W/cm^2 after irradiation for 0, 30, and 60 s is shown in Figure 4b. We further analyzed the photothermal destruction of the cells using the Arrhenius damage model (see the SI for details).[11] Fitting our measured values at the three laser intensities with the calculated damage parameter $\Omega(t)$ (Figure 4c) afforded the enthalpy and entropy values $\Delta H = 229 \pm 5$ kJ mol^{-1} and $\Delta S = 461 \pm 17$ J mol^{-1} K^{-1}, respectively (Figure 4c), which are consistent with the experimental relationship between ΔH and ΔS reported in the literature (Figure 4c inset).[11]

To visualize the damage process of cancer cells (Figure 4d), the distribution of gold nanocrosses associated with cells was imaged by their two-photon luminescence. At a lower laser intensity of ~1.3 W/cm^2, gold nanocrosses were found predominantly on the membranes of cells [Figure 4d(i)], and the cells remained almost unchanged in shape after 5 min of irradiation [Figure 4d(ii)]. At a higher laser intensity of 4.2 W/cm^2, cells started to shrink immediately upon laser exposure [Figure 4d(iii)]. After 30 s, cells had shrunk substantially in both

dx.doi.org/10.1021/ja202832r |J. Am. Chem. Soc. 2011, 133, 8506–8509

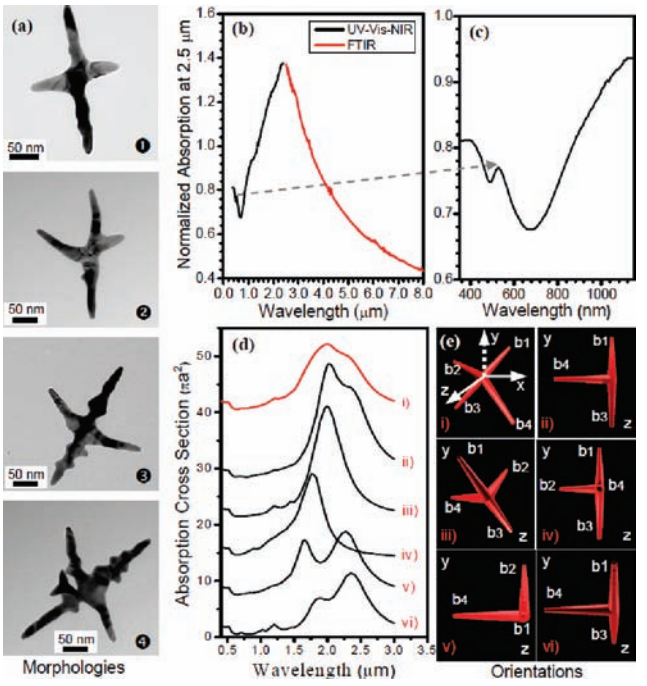

Figure 3. Near- and mid-IR absorption spectrum and DDA simulation of gold nanocrosses. (a) Images of four gold nanocrosses. (b) UV–vis–NIR absorbance in a spectral region ranging from the visible up to ~8 μm. (c) Pronounced near-IR absorption in the biological window. (d, e) Average simulated absorption spectrum [(i) in (d)] of the typical nanocross [(i) in (e)] obtained from the five simulated absorption spectra [(ii–vi) in (d)] corresponding to the five orientations [(ii–vi) in (e)]. The light was incident along the *x* axis and circularly polarized in the *yz* plane.

size and shape, and the collapsed cell membranes brought gold nanocrosses together to form agglomerates [Figure 4d(iv)]. The effective hyperthermia effect for killing cells was further theoretically investigated by simulating synergistic coupling among one, two, three, or four branches using DDA (Figure S3). When one of the branches is exposed to the incident polarized light along its long axis, the entire nanocross can be excited to participate in the light absorption. This property makes them useful as octopus antennas that efficiently capture incident IR light and convert it into heat for very fast photothermal destruction of cancer cells (see the SI for details).[12]

In summary, we have demonstrated a facile chemical synthesis of well-defined multiple-branched gold nanocrosses that exhibit a wide and pronounced surface plasmon resonance in the near- and mid-IR regions. The copper-induced formation of single or double twins leads to anisotropic growth of 2D and 3D gold nanocrosses along both ⟨110⟩ and ⟨001⟩ in a controlled fashion. The synergistic coupling between the branches allows the highly branched nanocrosses to efficiently capture IR light for effective photothermal destruction of cancer cells. The theoretical understanding and experimental demonstration of the enhanced hyperthermia properties of the gold nanocrosses together with the quantitative damage assessment of cells offer a very promising tool for use in tumor therapies. In addition to effective two-photon imaging and photothermal treatment, the near- and mid-IR gold nanocrosses may also find applications in IR sensing, thermal imaging, telecommunications, and the like.

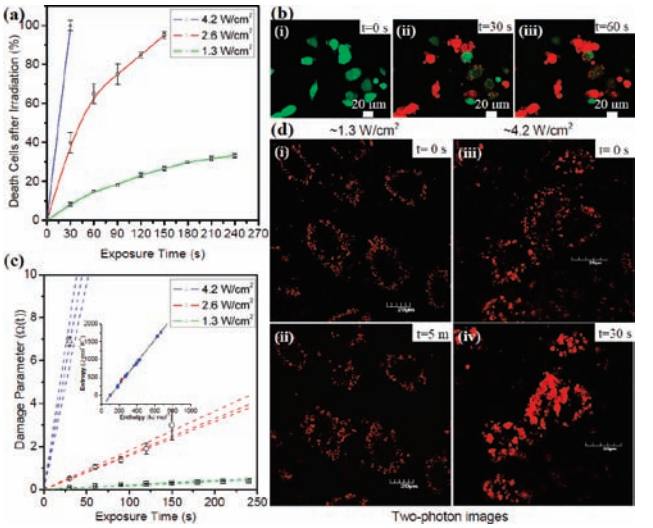

Figure 4. Photothermal damage, Arrhenius model, and two-photon luminescence imaging of A549 cancer cells associated with gold nanocrosses. (a) Photothermal damage as a function of time at 900 nm laser intensities of 1.3, 2.6, and 4.2 W/cm^2. (b) Confocal images showing the time-dependent damage process at 2.6 W/cm^2 after 900 nm irradiation for 0, 30, and 60 s. (c) Arrhenius damage model. Plots of the damage parameter $\Omega(t)$ as a function of laser exposure time at the three laser intensities are shown. The inset shows that the ΔH and ΔS values obtained from our data (red) are consistent with the experimental relationship reported in the literature (blue). (d) Two-photon luminescence images of gold nanocrosses associated with cells under 900 nm laser excitation at 1.3 and 4.2 W/cm^2.

■ ASSOCIATED CONTENT

Supporting Information. Experimental procedures, 3D tomography reconstruction, evaluation and modeling of the photothermal effect, details of the DDA simulations, and video clips (AVI). This material is available free of charge via the Internet at http://pubs.acs.org.

■ AUTHOR INFORMATION

Corresponding Author
adnen.mlayah@cemes.fr; my-han@imre.a-star.edu.sg

■ ACKNOWLEDGMENT

This work was financially supported by the Institute of Materials Research & Engineering, the National University of Singapore, and the CALMIP Computing Center at Paul Sabatier University of Toulouse.

■ REFERENCES

(1) (a) Tao, A. R.; Habas, S.; Yang, P. D. *Small* **2008**, *4*, 310–325. (b) Grzelczak, M.; Pérez-Juste, J.; Mulvaney, P.; Liz-Marzán, L. M. *Chem. Soc. Rev.* **2008**, *37*, 1783–1791. (c) Xia, Y. N.; Xiong, Y. J.; Lim, B. K.; Skrabalak, S. E. *Angew. Chem., Int. Ed.* **2009**, *48*, 60–103. (d) Halas, N. J. *Nano Lett.* **2010**, *10*, 3816–3822.

(2) (a) Jana, N. R.; Gearheart, L.; Murphy, C. J. *J. Phys. Chem. B* **2001**, *105*, 4065–4067. (b) Sun, Y. G.; Xia, Y. N. *Science* **2002**, *298*, 2176–2179. (c) Jin, R. C.; Cao, Y. W.; Mirkin, C. A.; Kelly, K. L.; Schatz, G. C.; Zheng, J. G. *Science* **2001**, *294*, 1901–1903. (d) Jin, R. C.; Cao, Y. C.; Hao, E. C.; Métraux, G. S.; Schatz, G. C.; Mirkin, C. A. *Nature* **2003**, *425*, 487–490. (e) Huang, X. Q.; Tang, S. H.; Mu, X. L.; Dai, Y.;

Chen, G. X.; Zhou, Z. Y.; Ruan, F. X.; Yang, Z. L.; Zheng, N. F. *Nat. Nanotechnol.* **2011**, *6*, 28–32.

(3) Hirsch, L. R.; Stafford, R. J.; Bankson, J. A.; Sershen, S. R.; Rivera, B.; Price, R. E.; Hazle, J. D.; Halas, N. J.; West, J. L. *Proc. Natl. Acad. Sci. U.S.A.* **2003**, *100*, 13549–13554.

(4) (a) Larsson, E. M.; Alegret, J.; Käll, M.; Sutherland, D. S. *Nano Lett.* **2007**, *7*, 1256–1263. (b) Skrabalak, S. E.; Chen, J. Y.; Sun, Y. G.; Lu, X. M.; Au, L.; Cobley, C. M.; Xia, Y. N. *Acc. Chem. Res.* **2008**, *41*, 1587–1595.

(5) Gansel, J. K.; Thiel, M.; Rill, M. S.; Decker, M.; Bade, K.; Saile, V.; Freymann, G. V.; Linden, S.; Wegener, M. *Science* **2009**, *325*, 1513–1515.

(6) (a) Liu, M.; Zentgraf, T.; Liu, Y. M.; Bartal, G.; Zhang, X. *Nat. Nanotechnol.* **2010**, *5*, 570–573. (b) Hendry, E.; Carpy, T.; Popland, M.; Mikhaylovskiy, R. V.; Lapthorn, A. J.; Kelly, S. M.; Barron, L. D.; Gadegaard, N.; Kadodwala, M. *Nat. Nanotechnol.* **2010**, *5*, 783–787. (c) Mirin, N. A.; Halas, N. J. *Nano Lett.* **2009**, *9*, 1255–1259. (d) Clark, A. W.; Glidle, A.; Cumming, D. R. S.; Cooper, J. M. *J. Am. Chem. Soc.* **2009**, *131*, 17615–17619. (e) Prodan, E.; Radloff, C.; Halas, N. J.; Nordlander, P. *Science* **2003**, *302*, 419–422.

(7) (a) Fan, J. A.; Wu, C. H.; Bao, K.; Bao, J. M.; Bardhan, R.; Halas, N. J.; Manoharan, V. N.; Nordlander, P.; Shvets, G.; Capasso, F. *Science* **2010**, *328*, 1135–1138. (b) Luk'yanchuk, B.; Zheludev, N. I.; Maier, S. A.; Halas, N. J.; Nordlander, P.; Giessen, H.; Chong, T. C. *Nat. Mater.* **2010**, *9*, 707–715.

(8) (a) Hao, F.; Nehl, C. L.; Hafner, J. H.; Nordlander, P. *Nano Lett.* **2007**, *7*, 729–732. (b) Nehl, C. L.; Liao, H. W.; Hafner, J. H. *Nano Lett.* **2006**, *6*, 683–688. (c) Chen, S. H.; Wang, Z. L.; Ballato, J.; Foulger, S. H.; Carroll, D. L. *J. Am. Chem. Soc.* **2003**, *125*, 16186–16187.

(9) (a) Huang, X. H.; El-Sayed, I. H.; Qian, W.; El-Sayed, M. A. *J. Am. Chem. Soc.* **2006**, *128*, 2115–2120. (b) Jain, P. K.; Huang, X. H.; El-Sayed, I. H.; El-Sayed, M. A. *Acc. Chem. Res.* **2008**, *41*, 1578–1586. (c) Qian, X. M.; Peng, X. H.; Ansari, D. O.; Yin-geon, Q. Q.; Chen, G. Z.; Shin, D. M.; Yang, L.; Young, A. N.; Wang, M. D.; Nie, S. M. *Nat. Biotechnol.* **2008**, *26*, 83–90. (d) Yavuz, M. S.; Chen, Y. Y.; Chen, J. Y.; Cobley, C. M.; Zhang, Q.; Rycenga, M.; Xie, J. W.; Kim, C. H.; Song, K. H.; Schwartz, A. G.; Wang, L. V.; Xia, Y. N. *Nat. Mater.* **2009**, *8*, 935–939. (e) Jin, Y. D.; Gao, X. H. *Nat. Nanotechnol.* **2009**, *4*, 571–576. (f) Matteini, P.; Ratto, F.; Rossi, F.; Centi, S.; Dei, L.; Pini, R. *Adv. Mater.* **2010**, *22*, 4313–4316.

(10) Tripathy, S.; Marty, R.; Lin, V. K.; Teo, S. L.; Ye, E. Y.; Arbouet, A.; Saviot, L.; Girard, C.; Han, M. Y.; Mlayah, A. *Nano Lett.* **2011**, *11*, 431–437.

(11) Jacques, S. L. *J. Biomed. Opt.* **2006**, *11*, No. 041108.

(12) Baffou, G.; Girard, C.; Quidant, R. *Phys. Rev. Lett.* **2010**, *104*, No. 136805.